

X-RAY LINE EMISSION FROM THE HOT STELLAR WIND OF θ^1 ORIONIS C

N. S. SCHULZ, C. R. CANIZARES, D. HUENEMOERDER, AND J. C. LEE

Center for Space Research, Massachusetts Institute of Technology, 70 Vassar Street, Cambridge, MA 02139

Received 2000 August 18; accepted 2000 October 16; published 2000 December 13

ABSTRACT

We present a first emission-line analysis of a high-resolution X-ray spectrum of the stellar wind of θ^1 Ori C obtained with the High-Energy Transmission Grating Spectrometer on board the *Chandra X-Ray Observatory*. The spectra are resolved into a large number of emission lines from H- and He-like O, Ne, Mg, Si, S, Ar, and Fe ions. The He-like Fe xxv and Li-like Fe xxiv appear quite strong, indicating very hot emitting regions. From H/He flux ratios as well as from Fe He/Li emission measure ratios, we deduce temperatures ranging from 0.5 to 6.1×10^7 K. The He triplets are very sensitive to density as well. At these temperatures the relative strengths of the intercombination and forbidden lines indicate electron densities well above 10^{12} cm $^{-3}$. The lines appear significantly broadened, from which we deduce a mean velocity of 770 km s $^{-1}$ with a spread between 400 and 2000 km s $^{-1}$. Along with results of the deduced emission measure, we conclude that the X-ray emission could originate in dense and hot regions with a characteristic size of less than 4×10^{10} cm.

Subject headings: binaries: general — stars: early-type — stars: winds, outflows — techniques: spectroscopic — X-rays: stars

1. INTRODUCTION

X-ray spectra from stellar winds have been quite difficult to interpret, since the first observations with *Einstein* (Seward et al. 1979). The spectral resolution from previous X-ray missions was insufficient for resolving any emission and absorption lines. Models that describe the mass loss from a hot luminous star successfully in the UV (Pauldrach et al. 1994; Lamers et al. 1999) could never correctly predict observed X-ray fluxes. A model involving a possible hot corona seems unlikely due to the lack of evidence for absorption at the 20.6 Å K shell ionization edge from oxygen (Cassinelli & Swank 1983); in addition, no coronal line emission (i.e., Fe xiv at 530 nm) was found in optical spectra of η Ori and κ Ori (Nordsieck, Cassinelli, & Anerson 1981) or in the prototype star for stellar winds in ζ Pup (Baade & Lucy 1987). X-ray emission from shocks emerging in instabilities within a radiatively driven wind forming a forward shock was proposed by Lucy & White (1980) and Lucy (1982). However, reverse shocks that decelerate material as it rams into dense shells ahead seem more likely (Owocki, Castor, & Rybicki 1988). These models predict X-rays up to a temperature of about $kT \sim 0.5$ keV. Feldmeier et al. (1997a, 1997b) introduced turbulent perturbations into their calculations, which ultimately allowed for higher temperatures.

Several recent observations with the 0.1–10.0 keV *ASCA* bandpass, i.e., of τ Sco (Cohen, Cassinelli, & Waldron 1997) and η Car (Tsuboi et al. 1997), indicated that there is a hard component to these spectra at greater than 2 keV. Although these two examples tend to resemble quite extreme cases of massive stars, *ASCA* observations of other, less massive O stars (Corcoran et al. 1994) and the Orion Trapezium (Yamauchi et al. 1996) indicated the existence of a similar hard component in their spectra as well. In the most recent analysis of *Chandra* CCD spectra of the Orion Trapezium, Schulz et al. (2000) were able to resolve the entire Trapezium into individual sources. Identified O and B stars showed a soft component at ~ 0.8 keV as observed with *ROSAT*; the very early spectral types required an additional hard component of temperatures above 2 keV as well.

In this Letter we present first results from an observation of θ^1 Ori C with the High-Energy Transmission Grating Spectrometer (HETGS; C. R. Canizares et al. 2000, in preparation)

on board *Chandra* (Weisskopf, O’Dell, & van Speybroeck 1996). We present an X-ray line list of the brightest emission lines detected and investigate emission-line properties to determine the range of temperatures and densities of the line-emitting regions. Some of the results will have immediate impact constraining models of stellar winds.

2. CHANDRA OBSERVATIONS AND DATA REDUCTION

θ^1 Ori C was observed with the HETGS on 1999 October 31 (05:47:21 UT) continuously for 53 ks. The HETGS carries two different types of transmission gratings, the Medium-Energy Grating (MEG) and the High-Energy Grating (HEG), with grating constants of 4000 and 2000 Å, respectively. It allows for high-resolution spectroscopy between 1 and 35 Å with a peak spectral resolution at 12 Å of $\lambda/\Delta\lambda \sim 1400$ and at 1.8 Å of $\lambda/\Delta\lambda \sim 180$ in first-order HEG spectra. The dispersed spectra were recorded with the Advanced CCD Imaging Spectrometer (G. P. Garmire et al. 2000, in preparation). We also refer to the available *Chandra* X-Ray Center (CXC) documents for more detailed descriptions.

We recorded a total of 4.5×10^4 events in the co-added first-order MEG spectra and 1.7×10^4 events in the HEG after standard grade selection. The level 1 event lists provided by the CXC were reprocessed using the latest available data processing input products. One of the major difficulties in the spectra extraction was that θ^1 Ori C is located in the core of the Orion Trapezium cluster, which has several sources that are bright enough to produce dispersed spectra as well as many X-ray sources in the vicinity, which then would imitate emission lines by coincidence. Most of these contributions can be removed by checking for dislocations of the source point-spread functions from the center of the cross-dispersion profile, by cross-correlating with each dispersion arm, and finally by the energy discrimination of the focal-plane CCDs.

In order to determine the zero point of the wavelength scale we fitted the dispersed images of the MEG and HEG and determined the intersections of these fits with the zero-order readout trace of the CCD. The fits of the MEG and HEG were consistent within 0.3 detector pixels (~ 0.003 Å in MEG and 0.002 Å in HEG first-order spectra). The current status of the overall wave-

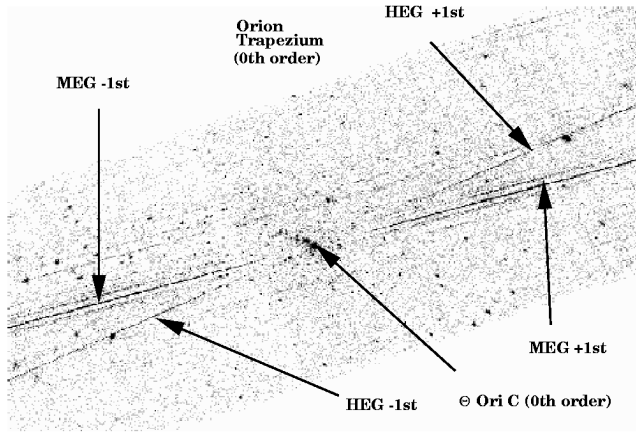


FIG. 1.—HETGS focal-plane image of the Orion Trapezium cluster

length calibration is of the order of 0.1% and mostly depends on uncertainties in the position of CCD gaps (± 0.5 pixels). This leads to a worst-case uncertainty in the scale of 0.01 \AA in first-order MEG spectra, 0.008 \AA in first-order HEG spectra, and 0.003 \AA in third-order MEG spectra. Level 1–1.5 event list processing as well as aspect-corrected exposure map computations were done using available CXC software, the final grating spectra were extracted using custom software and FTOOLS, and spectral fits were performed with ISIS.

3. HETGS SPECTRA

Figure 1 shows the focal-plane image of the Orion Trapezium cluster and its dispersed spectra. Several sources in the cluster are bright enough to produce highly resolved grating spectra. The brightest trace in the middle corresponds to θ^1 Ori C; arrows point to its zeroth-order image as well as the MEG and HEG spectral traces. The extracted and cleaned spectra are shown in Figure 2. The solid line shows the MEG co-added first-order spectrum, and similarly, the dotted line for the HEG. The spectral binning is 0.01 \AA . The spectra show a substantial continuum and numerous emission lines. At the current stage of analysis, we concentrate on relevant properties of the emission lines; global model fits will be left for subsequent papers.

3.1. Emission Lines

Table 1 displays the prominent set of lines, which for this analysis is the most interesting we have identified so far. We observe lines in a band from 1.8 to 19 \AA . There is not much flux above 22 \AA , since θ^1 Ori C is moderately absorbed with a column density of $1.93 \times 10^{21} \text{ cm}^{-2}$ (Schulz et al. 2000). The detected lines are from all major abundant elements, i.e., from H-like and He-like ions of O, Ne, Mg, Si, S, and Fe. Calcium and Argon lines are not apparent—they are either missing or below our statistical detection limits. The Ly α lines are strongly detected in all other species but Fe. For some ions we also observe the Ly β and higher transitions. In five ions—S, Si, Mg, Ne, and O—we resolve the He-like triplets into resonance (*r*), intercombination (*i*), and forbidden (*f*) lines. The Ne triplet is contaminated by Fe transitions. The triplet in Fe XXV is not resolved and the line appears considerably broadened. Iron is quite abundant, and in addition to many lower transitions, we observe strong lines from He-, Li-, and Be-like Fe. Here we only include Fe XXV and some lines from Fe XXIV

TABLE 1
EMISSION LINES FROM INNER SHELL IONS

Ion	Type	λ (Expected)	λ (Measured)	Flux ^a	FWHM ($\times 10^{-2} \text{ \AA}$)
Fe xxv	He4	1.851	1.856	7.533	3.07
Fe xxiv	Li2	7.987	7.984	2.596	3.17
S xvi	H2	3.990	3.997	1.458	2.31
S xvi	H1	4.730	4.729	6.141	1.46
S xv	He4	5.040	5.040	9.457	3.54
S xv	He5	5.060	5.060	2.734	0.13
S xv	He6	5.100	5.105	4.334	2.17
Si xiv	H2	5.220	5.218	3.913	3.34
Si xiv	H1	6.180	6.182	11.742	0.81
Si xiii	He4	6.650	6.650	7.313	1.11
Si xiii	He5	6.690	6.690	4.068	1.64
Si xiii	He6	6.740	6.740	5.579	1.63
Mg xii	H2	7.100	7.105	3.218	2.34
Mg xi	He2	7.470	7.466	2.100	2.51
Mg xii	H1	8.420	8.418	8.755	1.38
Mg xi	He4	9.170	9.169	3.000	1.65
Mg xi	He5	9.230	9.237	1.000	0.24
Mg xi	He6	9.310	9.316	0.600	...
Ne x	H4	9.480	9.474	5.834	...
Fe xxiv	Li6A	11.031	11.036	6.255	1.36
Fe xxiv	Li6B	11.184	11.178	5.879	0.35
Ne x	H1	12.130	12.145	12.950	3.47
Ne ix	He4	13.440	13.445	2.768	0.71
Fe xvii	Ne4	15.013	15.020	12.424	4.59
O viii	H2	16.010	16.019	2.441	4.63
O viii	H1	18.970	18.991	9.547	1.39
O vii	He4	21.600	21.600	1.428	0.24
O vii	He5	21.800	21.790	2.452	0.19

^a In units of $10^{-5} \text{ photons cm}^{-2} \text{ s}^{-1}$.

and Fe XVII, which we use for plasma diagnostics; a full investigation of the Fe lines is under way.

In order to determine line positions, widths, and fluxes we treated the underlying continuum as background and performed local fits using a generic flat model for the background and Gaussian functions for the lines. For the line identifications and nomenclature we use the line list presented by Mewe, Gronenschild, & van den Oord (1985). The wavelength identification is based on the closest known transition within the instrument resolution. Because of its superior resolution, line centroids below 13 \AA are determined using the HEG. The difference between the measured and expected line positions are well within the current uncertainties of the *Chandra* wavelength calibration; no obvious systematic shifts other than a trend for larger deviations at higher wavelength exists, which can be explained by the increasing uncertainty due to more CCD gaps in the dispersion direction.

3.2. Velocities

We mostly rely on the factor of 2 superior resolution of the HEG for line width measurements less than 13 \AA . These widths are shown in the sixth column of Table 1. Instrumental corrections have been applied using the latest HETGS response files. The most reliable widths come from the bright and unblended Ly α lines, where we consider the fine-structure splits negligibly small.

The FWHM of the lines range between 0.3 and $4.1 \times 10^{-2} \text{ \AA}$, an order of magnitude too large to be interpreted as thermal broadening. If we deduce Doppler velocities from $\Delta\lambda/\lambda = v_D/c$, we obtain a distribution of velocities with a mean value of 771 km s^{-1} (Fig. 3). The Fe XXV width at 1.85 \AA appears exceptionally wide, but we do not have the sensitivity

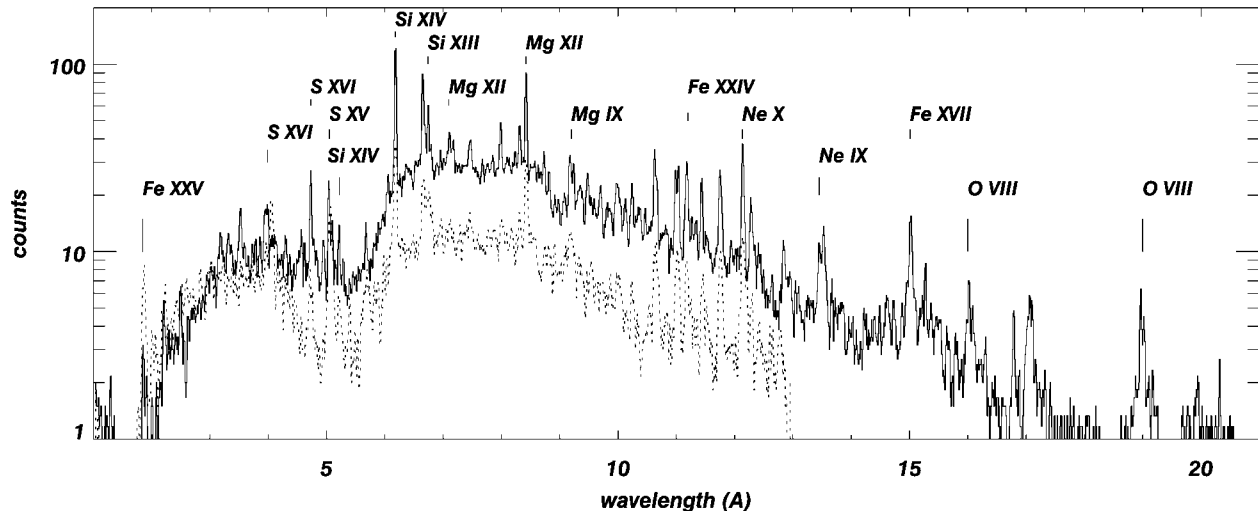


FIG. 2.—First-order MEG (solid line) and HEG (dotted line) count spectra

to resolve its r , i , and f components. However, if we force the fit using the triplet model, we obtain a mean width corresponding to a velocity of 1650 km s^{-1} . Near 11 \AA we also introduce systematic uncertainties by fitting weak as well as more blended lines, adding to an additional scatter in the observed line widths. The drop at 11 \AA , in that respect, may not be real. When we, for the time being, ignore these weaker data points, the velocity scatter is $\sim 400\text{--}2000 \text{ km s}^{-1}$. We do not observe any measurable asymmetries in the line shapes, which would indicate deviations from an isotropic wind emission geometry.

3.3. Temperatures and Electron Densities

Flux ratios of highly ionized ions are sensitive to the density and temperature of a collisionally ionized plasma (see Mewe 1999 for a review). We have several ways to estimate the local temperature from the line. We can use the $(f+i)/r$ flux ratio of the He-like triplet, the flux ratio of the H-like Ly α to the He-like resonance lines, as well as He- to Li-like and He- to Ne-like ion flux ratios. Comparing the line ratios with theory is difficult and depends on a variety of assumptions. Here we use the Astrophysical Plasma Emission Code and the corresponding database (APED¹) described by Smith et al. (1998). In general we make the assumption that for a specific transition the emitting plasma is isothermal or at least has a symmetric distribution with that peak temperature. We also assume that the emitting plasma is in ionization equilibrium. The ratios within the He-like triplets are good indicators for the local plasma temperature. A comparison of the flux ratios to calculated ratios from the database yields temperatures of $(4.2 \pm 3.1) \times 10^5 \text{ K}$ for O, $(9.3 \pm 3.8) \times 10^6 \text{ K}$ for Mg, $(2.0 \pm 1.4) \times 10^6 \text{ K}$ for Si, and $(1.5 \pm 1.1) \times 10^7 \text{ K}$ for S. The line flux ratios of the H- to He-like ions as well as the He- to Li-like Fe ions are good indicators of the temperature largely independent of density. Here the ratios for the Ly α transitions of O, Ne, Mg, Si, and S yield temperatures of (0.6 ± 0.2) , (0.7 ± 0.2) , (1.5 ± 0.2) , (2.0 ± 0.3) , and $(2.3 \pm 0.3) \times 10^7 \text{ K}$, respectively. The O, Ne, and Mg ratios have also been corrected for the effect of interstellar column density. Since we do not detect the Ly α line from Fe, we can

only set an upper limit to the temperature of $6.3 \times 10^7 \text{ K}$ by computing the ratio of its 3σ detection limit to the whole detected He-like Fe triplet. This limit is consistent with the results from the Li-like Fe lines, which predict temperatures between 3.5 and $5.1 \times 10^7 \text{ K}$. From the ratio with the Ne-like Fe XVII line, we deduce a lower temperature of $5.0 \times 10^6 \text{ K}$.

Although the uncertainties in the $(f+i)/r$ flux ratios are higher, since the ratio uses three relatively weak lines, the temperatures for O and Si are significantly lower than the ones deduced from the hydrogenic lines. In the case of Si this in part could be due to contamination of the forbidden line with the Mg XII Ly γ line. However, if we assume that we do not observe the Si XIII forbidden line at all, we deduce a temperature that is still a factor of 2 lower than the one from the hydrogenic lines. The fact that these temperatures are systematically lower could mean either that we are not in ionization equilibrium or, which we consider more likely, that part of the He-like and lower transitions originate from different, somewhat cooler zones.

The forbidden line intensity in the He-like triplets is metastable and thus density sensitive. However, it should also be noted that

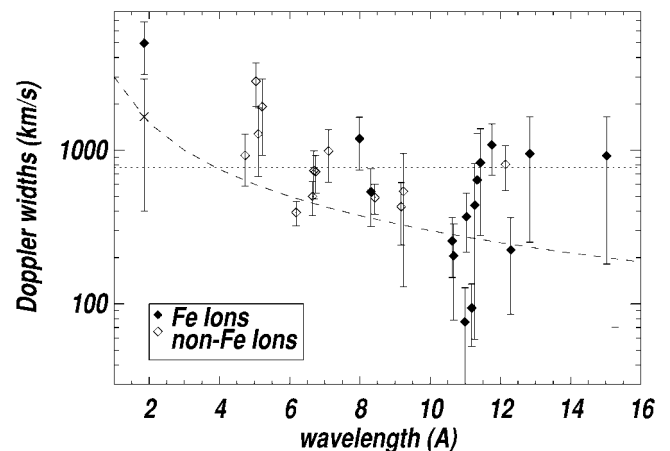


FIG. 3.—Instrument-corrected Doppler velocities deduced from fitted line widths. The dotted line shows the mean velocity; the dashed line shows the instrument width of the HEG.

¹ See <http://hea-www.harvard.edu/APEC>.

this ratio may also be affected by external radiation fields (Kahn et al. 2000). Here we simply compare the f/i ratio to the expectation from emissivity calculations from APED. In general, the ratios from elements of higher Z than Si are not suited for this analysis because here the ratio is not very sensitive to densities below 10^{15} cm^{-3} , which we do not expect. From the database, we deduce a lower density sensitivity limit of the f/i ratio to roughly 10^{10} cm^{-3} for O, 10^{12} cm^{-3} for Mg, and 10^{13} cm^{-3} for Si. For these ions we measure f/i ratios of 0.04 ± 0.02 , 0.60 ± 0.18 , and 1.37 ± 0.51 , corresponding to electron densities of $(3.5 \pm 2.7) \times 10^{12} \text{ cm}^{-3}$ for oxygen, $(4.3 \pm 2.3) \times 10^{13} \text{ cm}^{-3}$ for Mg, and $(9.0 \pm 10.6) \times 10^{13} \text{ cm}^{-3}$ for Si. We fixed the temperature to the ones obtained from the hydrogenic lines, because the latter lines are less density sensitive and we also assume that they are not affected by opacity effects. The uncertainties reflect the average upper and lower density limits according to the errors in the ratios. The O ratio is a lower limit, because as a result of not observing the forbidden line, we estimated the flux based on a 3σ detection limit. We observe a significant flux in the Mg XII Ly β line, which makes it very likely that the forbidden line in Si at 6.74 Å is contaminated with a Mg XII Ly γ line. From APED we calculated a emissivity ratio of the Mg XII Ly β to Ly γ of 3.05. Based on the observed flux for the Ly β line we can then estimate the flux contribution of the Mg XII Ly γ line to the Si XIII forbidden line. The f/i ratio in Si reduces then from 1.37 to 1.11.

Using the lines in Table 1 we also deduced volume emission measures (VEMs) assuming isothermal and isotropic conditions. We obtain the lowest VEM from Fe XVII with $1.52 \times 10^{54} \text{ cm}^{-3}$ and the highest from S XVI with $2.5 \times 10^{56} \text{ cm}^{-3}$. If we apply the deduced range of densities above and spherical geometry we find characteristic emission sizes between 4.0×10^8 and $3.9 \times 10^{10} \text{ cm}$.

4. DISCUSSION

A large number of emission lines were detected with a signal-to-noise ratio greater than 5σ . These lines are from H- and He-like ion species of Fe, S, Si, Mg, Ne, and O; Ca and Ar are not detected. We do not observe any residual line shifts we could attribute to the source.

The X-ray lines appear significantly broadened, implying a mean shock velocity of 770 km s^{-1} . A similar shock velocity of 500 km s^{-1} has been determined from *ROSAT* fits of ζ Pup spectra (Hillier et al. 1993). Within the statistical uncertainties and the current state of the analysis, the line profiles appear symmetric, showing blue- and redshifts of equal proportions. We therefore conclude that the wind emission is quite isotropic. Our estimates from the VEM indicates that the emission volume is

equivalent to a volume well within 1 stellar radius. However, simulations by Feldmeier et al. (1997b) indicated that the X-ray emission must extend far out into the wind. Estimating the distance of the X-ray-producing shell collision, we use the β velocity law (with $\beta = 0.88$) and a terminal velocity of $\sim 1000 \text{ km s}^{-1}$ (Prinja, Barlow, & Howarth 1990) to determine the distance where the wind reaches 770 km s^{-1} , which gives about 4 stellar radii. In this respect, it is plausible that the X-ray-emitting regions appear in very thin dense shells as described by Feldmeier et al. (1997b). Their model, however, predicts strong variability of the X-ray emission, which, at least in terms of total X-ray flux, is not observed during our observations.

Whatever the actual emission geometry turns out to be, the emitting regions of θ^1 Ori C appear well confined, hot, and dense, with temperatures ranging between 0.05 and $6 \times 10^7 \text{ K}$ (0.06–4.5 keV) and densities above 10^{12} cm^{-3} . CCD spectra of θ^1 Ori C already indicated that the X-ray emission must have a hot component with a temperature of $kT \sim 3 \text{ keV}$ (Yamauchi et al. 1996; Schulz et al. 2000), or equivalent to $\sim 4 \times 10^7 \text{ K}$. In a broadband study ranging from UV to *ASCA* spectra of the B0 V star τ Sco, Cohen (1996) also suggested that a wide range of temperatures up to 10^7 K is necessary to describe X-ray and UV emission. It is quite hard to explain such high temperatures with the line-driven shock instability models (Lucy & White 1980; Lucy 1982), which predict temperatures more on the order of $5 \times 10^6 \text{ K}$. The spectrum in Figure 2 also shows that the hard part of the spectrum cannot be explained by inverse Compton scattering of UV photons (Chen & White 1991), since it shows emission lines with characteristics similar to the low-energy lines. The approach by Feldmeier et al. (1997b) seems to provide promising ingredients for describing the coexistence of low and high temperatures at relatively high densities. A more recent analysis by Kahn et al. (2000) of *XMM* Reflection Grating Spectrometer spectra of ζ Pup also resulted in low f/i line ratios and thus high density values, but it was suggested that a high UV radiation field could destroy the He-like forbidden line, leading to an overestimation of the density.

It still remains to be explained whether the high temperatures in θ^1 Ori C and other hot candidates are the exception or the rule. Clearly, we need more high-resolution X-ray observations of massive O stars in order to classify the X-rays in terms of their line emission properties. These properties include temperature ranges, densities, emission volumes, and ionization balance.

The authors want to thank N. Brickhouse for providing additional atomic data tables and the *Chandra* X-Ray Center for its enormous support. This research is funded by contracts SV-61010 and NAS8-39073.

REFERENCES

- Baade, D., & Lucy, L. B. 1987, *A&A*, 178, 213
 Cassinelli, J. P., & Swank, J. H. 1983, *ApJ*, 271, 681
 Chen, W., & White, R. L. 1991, *ApJ*, 366, 512
 Cohen, D. H. 1996, *PASP*, 108, 1140
 Cohen, D. H., Cassinelli, J. P., & Waldron, W. L. 1997, *ApJ*, 488, 397
 Corcoran, M. F., et al. 1994, *ApJ*, 436, L95
 Feldmeier, A., Kudritzki, R. P., Palsa, R., Pauldrach, A. W., & Puls, J. 1997a, *A&A*, 320, 899
 Feldmeier, A., Puls, J., & Pauldrach, A. W. 1997b, *A&A*, 322, 878
 Hillier, D. J., Kudritzki, R. P., Pauldrach, A. W., Baade, D., Cassinelli, J. P., Puls, J., & Schmitt, J. H. M. M. 1993, *A&A*, 276, 117
 Kahn, S. M., Leutenegger, M. A., Cottam, J., Rauw, G., Vreux, J. M., den Boggende, A. J., Mewe, R., & Guedel, M. 2000, *A&A*, submitted
 Lamers, H. J. G. L. M., Haser, S., de Koter, A., & Leitherer, C. 1999, *ApJ*, 516, 872
 Lucy, L. B. 1982, *ApJ*, 255, 286
 Lucy, L. B., & White, R. L. 1980, *ApJ*, 241, 300
 Mewe, R. 1999, in *X-Ray Spectroscopy in Astrophysics*, ed. J. van Paradijs & J. A. M. Bleeker (New York: Springer), 109
 Mewe, R., Gronenschild, E. H. B. M., & van den Oord, G. H. J. 1985, *A&AS*, 62, 197
 Nordieck, K. H., Cassinelli, J. P., & Anderson, C. M. 1981, *ApJ*, 248, 678
 Owocki, S. P., Castor, J. I., & Rybicki, G. B. 1988, *ApJ*, 335, 914
 Pauldrach, A. W., Kudritzki, R. P., Puls, J., Butler, K., & Hunsinger, J. 1994, *A&A*, 283, 525
 Prinja, R. K., Barlow, M. J., & Howarth, I. D. 1990, *ApJ*, 361, 607
 Schulz, N. S., Canizares, C. R., Huenemoerder, D., Kastner, J., & Taylor, S. 2000, *ApJ*, in press
 Seward, F. D., Forman, W. R., Giacconi, R., Griffiths, R. E., Harnden, F. R., Jr., Jones, C., & Pye, J. P. 1979, *ApJ*, 234, L55

Smith, R. K., Brickhouse, N. S., Raymond, J. C., & Liedahl, D. A. 1998, in Proc. First *XMM* Workshop, Science with *XMM*, ed. M. Dahlem (Noordwijk: ESA)

Tsuboi, Y., Koyama, K., Sakano, M., & Petre, R. 1997, *PASJ*, 49, 85

Weisskopf, M. C., O'Dell, S. L., & van Speybroeck, L. P. 1996, *Proc. SPIE*, 2805, 2

Yamauchi, S., Koyama, K., Sakano, M., & Okada, K. 1996, *PASJ*, 48, 719